Measurement 116 (2018) 264–272

Contents lists available at ScienceDirect

Measurement

journal homepage: www.elsevier.com/locate/measurement

An evaluation of the anticorrosion effect of ethylene glycol for AA7075-T6 alloy in 3.5% NaCl solution

Hüsnü Gerengi[a,*], Moses M. Solomon[a], Ertuğrul Kaya[a], Fatma E. Bagci[a], Ekaette J. Abai[b]

[a] Corrosion Research Laboratory, Department of Mechanical Engineering, Faculty of Engineering, Duzce University, 81620 Duzce, Turkey
[b] Department of Science Technology, Akwa Ibom State Polytechnic, Ikot Osurua, Ikot Ekpene, Akwa Ibom State, Nigeria

ARTICLE INFO

Keywords:
AA7075-T6 alloy
NaCl solution
Corrosion
Ethylene glycol
Corrosion inhibition
DEIS

ABSTRACT

The corrosion behaviour of AA7075-T6 aluminum alloy in 3.5% NaCl devoid of and containing various amounts of ethylene glycol (EG) has been examined by DEIS (dynamic electrochemical spectroscopy), PDP (Potentiodynamic polarization), SEM (scanning electron microscope), EDAX (energy dispersive X-ray spectroscopy), and AFM (atomic force microscope). AA7075-T6 alloy specimen corroded significantly in 3.5% NaCl solution. In 3.5% NaCl containing EG, the alloy is protected but the extent of protection is a function of immersion duration and concentration of EG. EG affects both the anodic and cathodic corrosion reactions according to PDP results. The adsorption of EG molecules onto AA7075-T6 surface follow Langmuir adsorption isotherm model. The ΔG^0_{ads} value calculated for the adsorption process reveals that physisorption is the prevailing mechanism. SEM and AFM pictures support the experimental results and EDAX results confirm the presence of EG molecules on AA7075-T6 surface.

1. Introduction

AA7075 is an alloy of aluminum with Zn, Mg, and Cu as the alloying elements. Notable characteristics of this alloy include high strength, excellent ductility, toughness, and high fatigue. Depending on the heat treatment, AA7075 is differentiated into 7075-0, 7075-T6, 7075-T651, 7075-T7, 7075-T73, and 7075-RRA. Compared with other grades, the AA7075-T6 has higher strength and better machinability and thus gains wider application in aerospace, automobile, and construction industries [1]. Nevertheless, the AA7075 alloy is susceptible to different forms of corrosion. Localized [2], pitting [3,4], and intergranular [5,6] forms of corrosion of AA7075 had been reported.

Glycols are organic compounds which have attracted great attention owing to their low volatility and viscosity, good electrical conductivity and heat transfer capacity, remarkable hydrophobicity and miscibility with polar solvents, as well as low cost [7]. They are used as an antifreezing, dehydrating, and cooling agent as well as chemical intermediate [8]. They also gain application as heat transfer fluid and as solvent [8]. Ethylene glycol (EG), a colourless, odourless, and sweet tasting syrup is the second member of this family and is deemed most essential [7] because of its moderate toxicity compared to others. One of its uses is as a coolant in engines [9,10]. It is known that engine coolants are often contaminated by chlorides and as effect induce the corrosion of metals used in the coolant system [9]. The dissolution of metals in EG-water solution have been studied. Fekry and Fatayerji [10] investigated inhibitor concentration effect on the dissolution pattern of AZ91D Mg alloy in EG-water solution using electrochemical approaches. They found that the rate of dissolution of the metal varied inversely with EG concentration. Santambrogio et al. [7] studied the influence of degradation acid products of EG-water solution (glycolic, formic, acetic, and oxalic acids) on the corrosion pattern of low carbon steel. The authors noted that the nature and relative proportion of the carboxylic acids detect the level of deteroriation of the metal in the studied environment. Khomami et al. [11] examined the effect of rotating speed on the electrochemical properties of steel alloy specimen in EG-water solutions and concluded that the corrosion rate of the specimen was not significantly changed by rotating speed. Most recently, Medhashere and Shetty [9] assessed the corrosion of Mg-Al-Zn-Mn alloy in EG-water solution enriched with chloride ions. They documented that the corrosion rate of the alloy varied directly with the amount of chloride ions and system temperature.

In this work, we deploy dynamic electrochemical spectroscopy (DEIS) to track the changes in the electrochemical properties of AA7075-T6 alloy in 3.5% NaCl solution free from and enriched with different amounts of EG with time. The DEIS which is an optimized method for impedance studies of corrosion processes in galvanostatic-time domain mode is best suited for corrosion and corrosion inhibition measurements because; corrosion process is dynamic in nature [12].

* Corresponding author.
E-mail address: husnugerengi@gmail.com (H. Gerengi).

https://doi.org/10.1016/j.measurement.2017.11.030
Received 12 July 2017; Received in revised form 4 October 2017; Accepted 13 November 2017
Available online 14 November 2017

Table 1
Chemical compositions of working electrode (wt%).

Sample	Zn	Mg	Fe	Si	Cu	Al
AA7075-T6	5.81	2.55	0.21	0.008	1.67	89.752

The PDP curves of this alloy in the NaCl-EG solutions have also been obtained. Surface examination of the exposed alloy is achieved using SEM and EDAX respectively.

2. Experimental

2.1. Specimens and medium

The alloy specimens utilized in the investigation were made from AA7075-T6 aluminum alloy sheet which was supplied by Erdemir Steel Co.,Turkey. The alloy has the chemical composition given in Table 1. The medium studied was 3.5% NaCl solution prepared from analytical grade NaCl pellets. The concentrations of ethylene glycol added to the corrosive medium were 10%, 20%, 30%, 40%, and 50%. Distilled water was used in all preparations. The EG and other chemicals used in the study were of AR and were used as procured.

2.2. DEIS measurements

This set of experiments were performed utilizing a National Instrument Ltd PCI-4461 digital-analog card. This card was equally used in recording the current and voltage perturbation of the investigated environment. Fig. 1 shows a generalized form of the DEIS set-up. All experiments were undertaken under galvanostatic condition achieved using an Autolab HGMEM-01 equipment. This equipment also serve as a current-voltage converter. A package of about 20 elementary current sinusoids was the source of perturbation signal. The frequency range of perturbation was 4.5 kHz to 300 mHz and the perturbation amplitude of 10 mV was utilized through out the measurements. A more detailed information on the use of DEIS under galvanostatic condition can be found in Slepski et al. [12]. The obtained DEIS spectra were analyzed using a ZsimpWin 3.21 software.

2.3. PDP measurements

An application software DC105 embedded in a Gamry instrument potentiostat/galvanostat/ZRA (Reference 600) was used for PDP experiments. The electrochemical assembly is a tri-electrode type with a silver/silver chloride glass as the reference electrode, a platinum mesh as the counter electrode and the AA7075-T6 specimen as the working electrode. Before the AA7075-T6 sample was used as the working electrode, it was subjected to mechanical abrasion. Emery papers of various grades (600, 800, 1500 and 2000) were used in the abrasion process. The abraded sample was washed in running water and ethanol and then dried in acetone in order to remove the dust generated from the abrasion. The working electrode was scanned starting from the cathodic direction to anodic direction at a rate of 1 mV/s in the potential range of −250 to +250 mV relative to corrosion potential (E_{corr}). To obtain the electrochemical polarization parameters, the PDP curves were extrapolated as described by Hefni et al. [13].

2.4. SEM and EDAX characterization

After DEIS experiments, the AA7075-T6 samples were submitted for SEM and EDAX analysis. Before the submission, the retrieved specimens were allowed to dry at ordinary temperature. The surface analysis was done on a Quanta FEG 250 scanning electron microscope (FEI, The

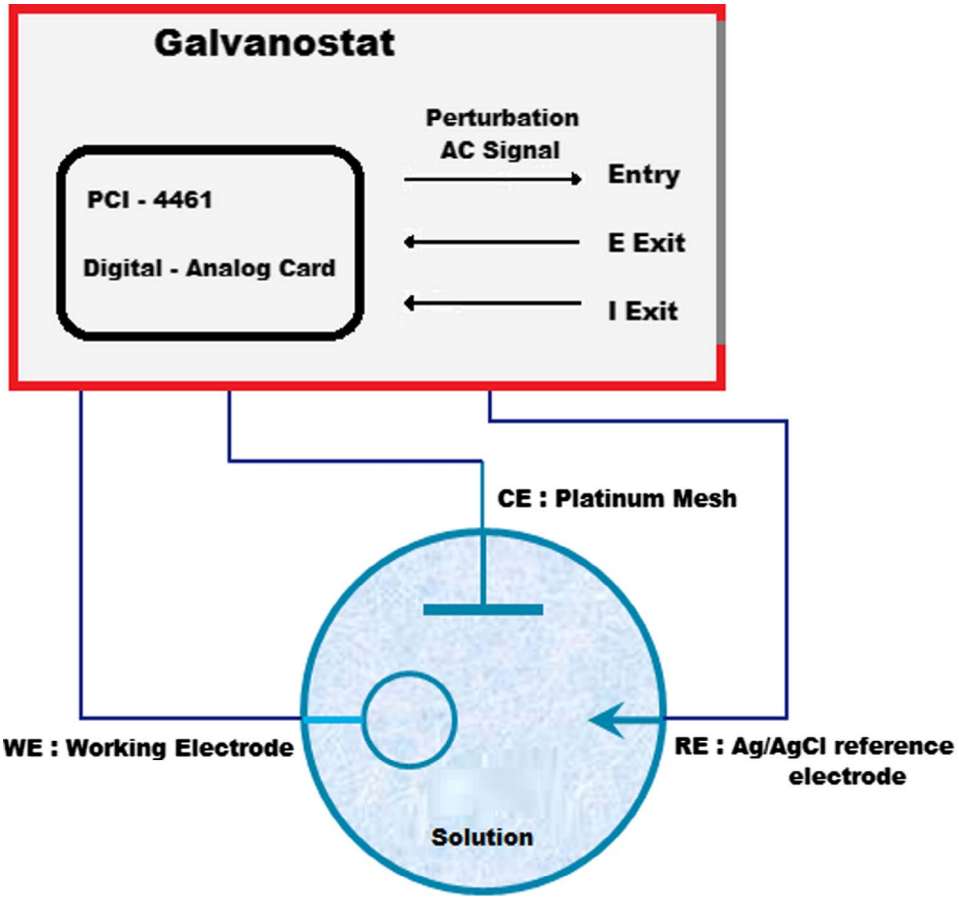

Fig. 1. General view of DEIS setup.

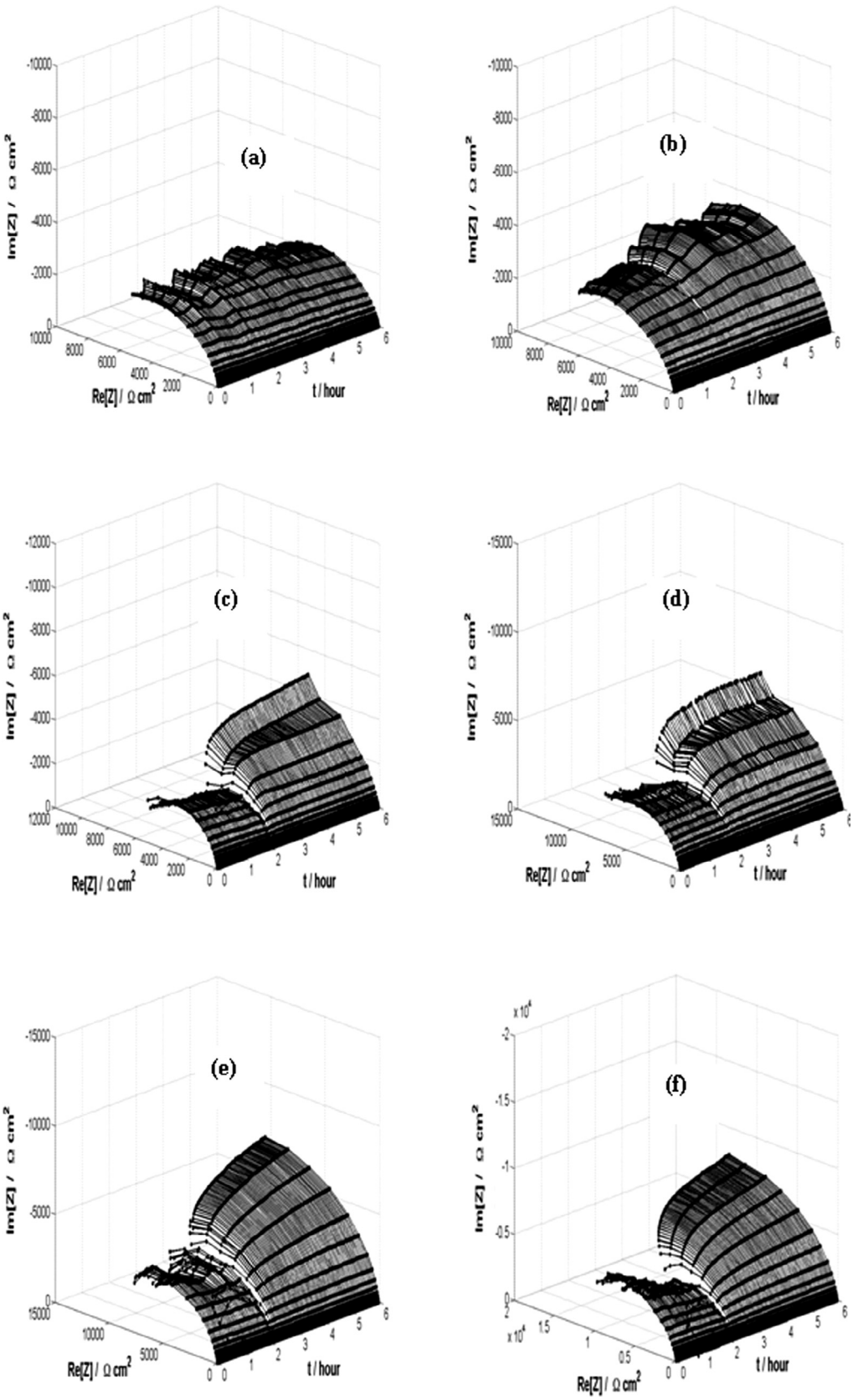

Fig. 2. DEIS spectra of AA7075-T6 aluminum alloy recorded in 3.5% NaCl solution (a) without and with (b) 10%, (c) 20%, (d) 30%, (e) 40%, and (f) 50% ethylene glycol for 6 h at 25 °C.

Netherlands) coupled with a probe for elemental composition measurement.

3. Results and discussion

3.1. DEIS studies

Instantaneous corrosion progress on a metal surface in a changing environment can be accurately track using DEIS. Fig. 2 shows the DEIS spectra recorded for AA7075-T6 alloy specimen immersed in 3.5% NaCl solution free of and enriched with various amounts of EG for 6 h at ordinary temperature. Notable features of the spectra are: (i) in all cases, the spectra are semi-circular in shape inferring that the corrosion of the metal substrate in the studied environment is controlled by charge transfer [14]; (ii) the semi-circular is continuous spanning through the time of measurement. This means that the metal sample will corrode as long as it remains in the investigated environment. (iii) The semicircles are not perfect. The imperfectness usually referred to as 'frequency dispersion phenomenon' [15,16] could arise due to the heterogenous nature of the working electrode surface. (iv) At point of introduction of EG into the corrosive solution (2 h), there is a disconnection and the size of the semicircle becomes bigger (Fig. 2b–f). This may mean stiff resistance to the flow of electron on the specimen surface which can be caused by the adsorption of EG molecules onto the surface. (v) The increase in the size of the semicircular graph is concentration dependent suggesting larger surface coverage by hydrophobic film formed by EG. (vi) It appears from close inspection that size of the spectra in Fig. 2b-f is directly proportional to immersion time. This could be possible if more of EG molecules are adsorbed on the AA7075-T6 surface as time elapses and also if the adsorbed film is more stable at longer time.

To better understand the changes in the charge transfer resistance (R_{ct}) on the metal surface as time of immersion progresses, a plot of R_{ct} against immersion time (t) is made (Fig. 3). It is interesting to see from the figure that R_{ct}-t graph for the metal in NaCl solution without EG first increases and reaches a peak at about 2500 s. At about 7200 s the R_{ct}-t graph assumes a steady plateau. This seems to reflect the protective tendency of the oxide layer on the Al alloy surface. Al is know to exhibit some form of resistance to corrosion [17–19]. However, this oxide layer may have been broken down as time prolonged resulting in the observed decline and steady plateau observed in the graph. Compared with the graphs representing the NaCl-EG systems, one could visibly see significant improvement on the charge transfer resistance of the metal surface occasioned by the presence of EG. The effect, as could be seem in Fig. 3 is a direct function of EG concentration and immersion time. It

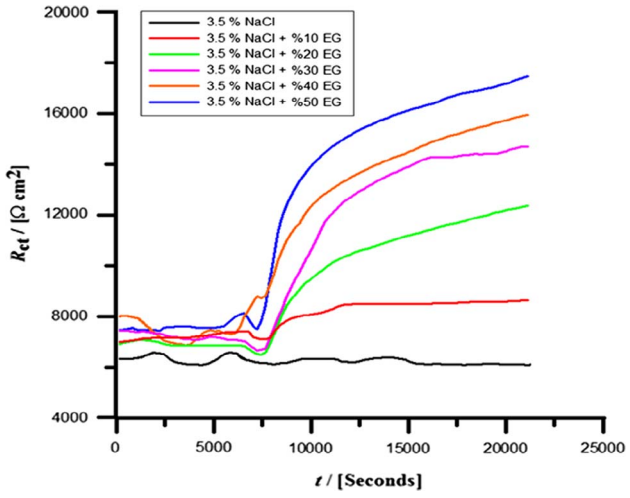

Fig. 3. Plot ofR_{ct}as a function of immersion time(s) for AA7075-T6 alloy in 3.5% NaCl solution in the absence and presence of of EG at 25 °C.

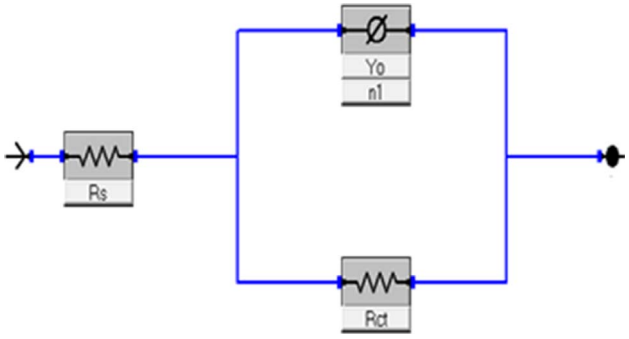

Fig. 4. Equivalent circuit model used to fit DEIS experimental data.

is obvious from this figure that EG in NaCl solution, particularly the higher concentration offered stiff opposition to the transfer of charge from the alloy surface.

To provide quantitative information on the corrosion of AA7075-T6 in the investigated environment and the extent of inhibition by EG, the DEIS spectra were analyzed utilizing $R_s(QR_{ct})$ equivalent circuit (Fig. 4). R_s denotes the solution resistance, R_{ct} charge transfer resistance while Q represents the constant phase element. Q is defined in impedance representation as:

$$Z_{CPE} = Y_0^{-1}(i\omega)^{-n} \quad (1)$$

where Y_0 is the Q constant, ω is the angular frequency (in rad s^{-1}), $i^2 = -1$ is the imaginary number and n is a Q exponent. The choice of this equivalent circuit was necessitated by the low chi square values and percentage error which did not exceed 5% through out the analysis. The quantitative information obtained from the analysis are presented in Table 2. The double-layer capacitance (C_{dl}) also given in Table 2 was calculated using Eq. (2) [20].

$$C_{dl} = (Y_0 R_{ct}^{1-n})^{1/n} \quad (2)$$

As clearly seen in the table, the solution resistance (R_s) and the R_{ct} values for the blank are smaller than those of the EG containing systems while the reverse is noted for the C_{dl} value. Increase in the amount of EG is seen to further cause in increase in the R_s and R_{ct} values and a decline in the C_{dl} value. For instance, the R_s and R_{ct} values for the NaCl solution devoid of EG are 8.78 Ω cm^2 and 5655 Ω cm^2 respectively while the C_{dl} value is 1.781 μF cm^2. When 10% EG was added to the considered aggressive solution, the R_s and R_{ct} values increased to 9.78 Ω cm^2 and 8664 Ω cm^2 respectively while the C_{dl} value decreased to 1.095 μF cm^2. By increasing the concentration of EG to 50%, the R_s and R_{ct} values further increase to 14.86 Ω cm^2 and 18,540 Ω cm^2 respectively and the C_{dl} value declined to 0.319 μF cm^2. This clearly shows that EG can act as inhibitor in chloride containing environment. The decline in C_{dl} value with increasing EG amount is in perfect conformity with the Helmholtz equation written as [21,22]:

$$\delta_{ads} = \frac{\varepsilon\varepsilon_o A}{C_{dl}} \quad (3)$$

where δ_{ads} = thickness of adsorbed layer, ε_o = permittivity of air, ε = local dielectric constant, and A = surface area of electrode.

The percentage protection ability (%IP) of EG in the studied environment was computed using Eq. (4):

$$\%IP = \left(1 - \frac{R_{ct}^0}{R_{ct}}\right) \times 100 \quad (4)$$

where R_{ct}^0 is the charge transfer resistance in the absence of EG and R_{ct} is the charge transfer resistance in the presence of EG. The values as presented in Table 2 are in perfect agreement with the qualitative results (Figs. 2 and 3) revealing that the inhibiting efficacy of EG is determined by the concentration used. The highest studied concentration (50%) of EG can protect AA7075-T6 surface in 3.5% NaCl solution by

Table 2
Dynamic electrochemical impedance parameters for AA7075-T6 alloy in 3.5% NaCl solution in the absence and presence of EG at 25 °C.

System/concentration	R_s (Ω cm^2)	Q		R_{ct} (Ω cm^2)	C_{dl} (μF cm^2)	%IP
		Y_0 ($\mu\Omega^{-1}$ S^n cm^{-2})	n $0 \le n \le 1$			
Blank	8.78	0.309	0.81	5655	1.781	–
3.5% NaCl + 10% EG	9.78	0.253	0.84	8664	1.095	35
3.5% NaCl + 20% EG	10.17	0.185	0.85	12420	0.725	54
3.5% NaCl + 30% EG	10.98	0.161	0.86	14600	0.570	61
3.5% NaCl + 40% EG	11.97	0.131	0.88	16030	0.372	65
3.5% NaCl + 50% EG	14.86	0.103	0.87	18540	0.319	70

70%.

Also given in Table 2 is the derived values for the parameter *n*. The parameter is often used as a gauge on the degree of roughness of the working electrode [15] and also the nature of the interface [21]. In our case, *n* value is in the range of 0.81–0.87. This value reflects a capacitive interface [15,21]. The *n* values for NaCl-EG systems are bigger than that representing the NaCl system implying that the alloy surface was rougher in NaCl-EG solutions than in NaCl solution [23]. Adsorption of EG molecules onto the alloy surface could give rise to the observation.

3.2. PDP studies

Fig. 5 illustrates the Potentiodynamic polarization curves obtained for AA7075-T6 aluminum alloy in 3.5% NaCl solution devoid of and containing 10–50% ethylene glycol at 25 °C. By extrapolating the linear segment of the anodic and cathodic branches, the electrochemical parameters namely, E_{corr} (corrosion potential), β_a (anodic potentiodynamic constant), β_c (cathodic potentiodynamic constant), and i_{corr} (corrosion current density) were derived. To get the percentage protection, the i_{corr} values were substituted into Eq. (5) [15]:

$$\%IP = \left(1 - \frac{i_{corr(EG)}}{i^0_{corr(blank)}}\right) \times 100 \quad (5)$$

All the obtained electrochemical polarization parameters are listed in Table 3. An inspection of the PDP graph obtained for AA7075-T6 in the free 3.5% NaCl solution reveals that the anodic branch exhibit long passive region. It is accepted that oxide film on Al surface formed

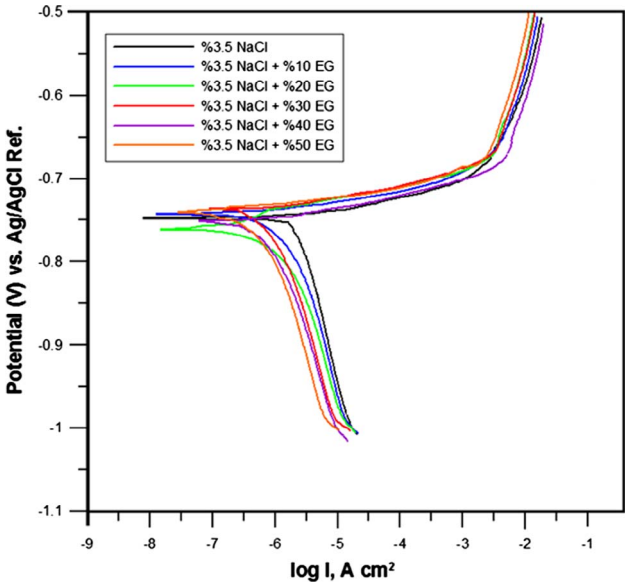

Fig. 5. Tafel polarization curves obtained for AA7075-T6 alloy in 3.5% NaCl solution in the absence and presence of EG at 25 °C.

Table 3
Potentiodynamic polarization parameters for AA7075-T6 alloy in 3.5% NaCl solution in the absence and presence of EG at 25 °C.

System/concentration	β_a (mV/dec)	β_c (mV/dec)	E_{corr} (mV)	I_{corr} (μA/cm^2)	%IP
Blank	22	315	−747	2.68	–
3.5% NaCl + 10% EG	21	260	−742	1.56	42
3.5% NaCl + 20% EG	19	246	8760	1.10	59
3.5% NaCl + 30% EG	15	238	−736	0.85	70
3.5% NaCl + 40% EG	17	206	−751	0.73	73
3.5% NaCl + 50% EG	18	198	−740	0.63	76

following Eqs. (6) & (7) offer some degree of protection against corrosion [24–26].

$$Al(s) + 3OH^- \rightarrow Al(OH)_{3,ads} + 3e^- \quad (6)$$

$$2Al(OH)_{3,ads} \rightarrow Al_2O_3 \cdot 3H_2O \quad (7)$$

However, in aggressive environment such as the one considered in this investigation, the oxide layer will be broken down and the bare metal surface attack by corrosive ions. In NaCl environment, the bare Al surface will undergo the following deteroriation reactions [24,25]:

$$Al \rightarrow Al^{3+} + 3e^- \quad (8)$$

$$Al^{3+} + 4Cl^- \rightarrow AlCl_4^- \quad (9)$$

Correspondingly, the reactions in Eqs. (10) and (11) will proceed at the cathodic side [25,27]:

$$1/2O_2 + H_2O + e^- \rightarrow OH_{ads} + OH^- \quad (10)$$

$$OH_{ads} + e^- \rightarrow OH^- \quad (11)$$

Interaction of adsorbed Cl^- ions with Al^{3+} in the oxide lattice forming oxychloride complex (Eq. (12)) had also been reported [24,27].

$$Al^{3+} + 2Cl^- + 2OH \rightarrow Al(OH)_2Cl_2^- \quad (12)$$

It is noted in Fig. 5 that the presence of EG in NaCl solution intercepted both the anodic and cathodic reactions but the principal effect seems to be on the cathodic reactions. For instance, the presence of 50% EG in the studied solution caused a marked decline in β_c value of the blank from 315 mV/Dec to 198 mV/Dec but only shifted the anodic slope value by 4 points (22 mV/Dec to 18 mV/Dec). In the system, EG is reduced thus [28]:

$$CH_2CH_2(OH)_2 + e^- \rightarrow OHCH_2CH_2O^- + H^+ \quad (13)$$

Our results suggest that Eq. (13) is preferred over Eqs. (10) and (11). The $OHCH_2CH_2O^-$ anions can also interrupt the formation of Al $(OH)_{3,ads}$ (Eq. (6)) as shown in Eq. (14) and by so doing protect the alloy surface against corrosive attack.

$$Al^{3+} + 3OHCH_2CH_2O^- \rightarrow Al(OHCH_2CH_2O)_3 \quad (14)$$

This inhibition which is found to depend on the concentration of EG used is reflected in the reduction of corrosion current and displacement

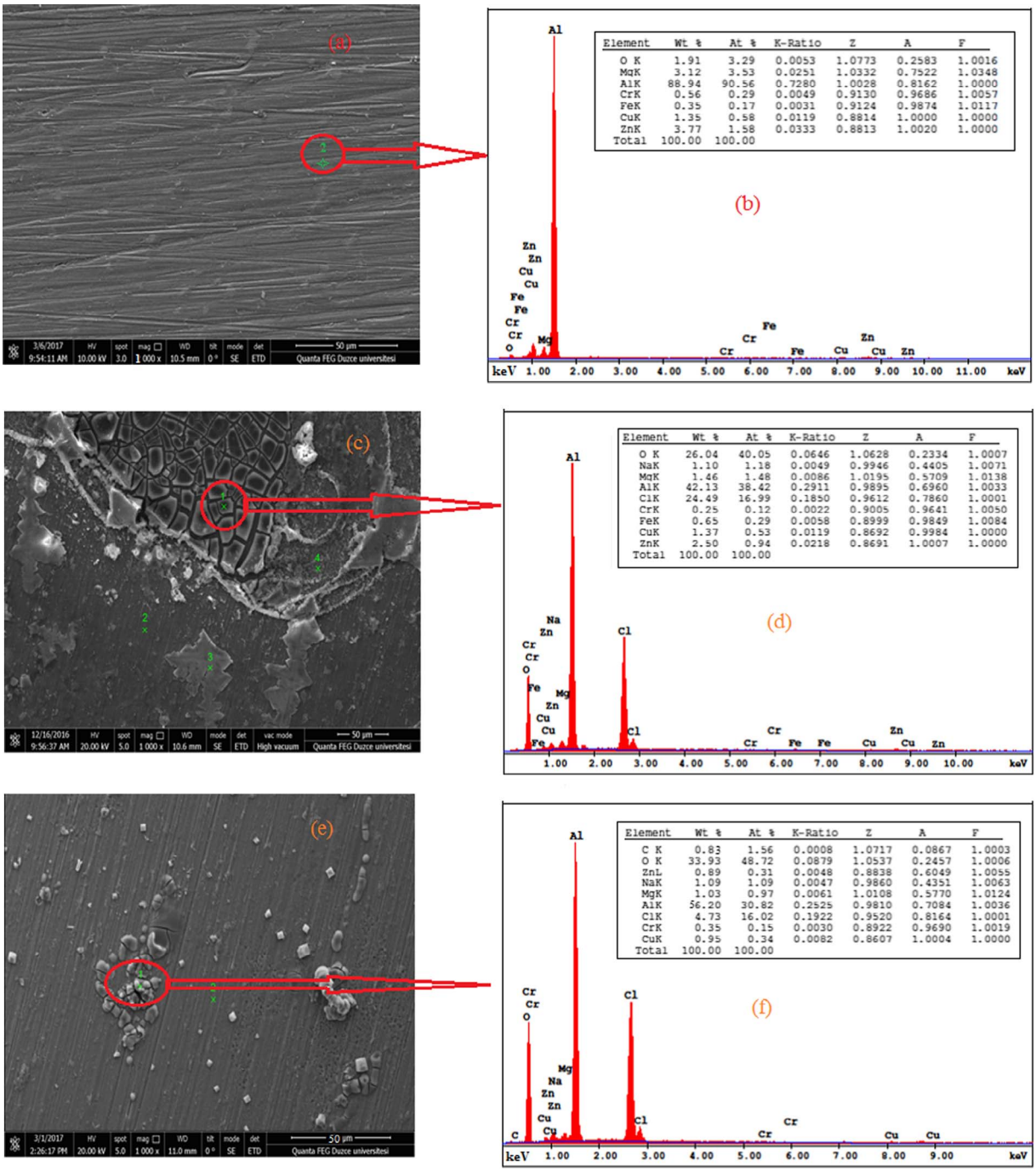

Fig. 6. SEM images and EDAX spectra for AA7075-T6 alloy in (a, b) abraded state, (c, d) exposed to 3.5% NaCl solution, and (e, f) exposed to 3.5% NaCl solution containing 50%EG after 6 h of immersion at 25 °C.

of E_{corr} toward more nobler position relative to the blank (Table 3). The highest protection efficiency achieved by 50% EG from this technique is 76%.

3.3. Surface assessments

3.3.1. SEM and EDAX investigations

Fig. 6 displays the SEM pictures and EDAX spectra obtained for AA7075-T6 aluminum alloy in (a, b) abraded form, (c, d) exposed to 3.5% NaCl solution, and (e, f) exposed to 3.5% NaCl solution containing 50% EG after 6 h of immersion at 25 °C. The arrows in Fig. 6(a), (c), and (e) show the portion of the specimen surfaces considered for EDAX analysis. The quantitative information derived from EDAX studies are inserted in the EDAX diagrams. The surface in Fig. 6(a) is well abraded giving rise to a very intensed Al peak in Fig. 6(b). The weight percentage of the Al peak is 88.94% (inserted table in Fig. 6(b)). When this specimen was immersed in 3.5% NaCl solution, it was destroyed due to attack by corrosive ions present in the solution. As could be seen in Fig. 6(c), the surface is covered with corrosion products. The corresponding EDAX spectrum (Fig. 6(d)) reveals that the corrosion products are mainly chlorides and oxides thereby agreeing with Eqs. (9) & (10). From the inserted table in Fig. 6(d), the percentage content of oxygen increased from 1.91% in the abraded surface to 26.04% while the chloride ions content on the surface stands at 24.49%. The information in the table inserted in Fig. 6(f) discloses that, in NaCl + EG solution, adsorbed EG molecules displaces

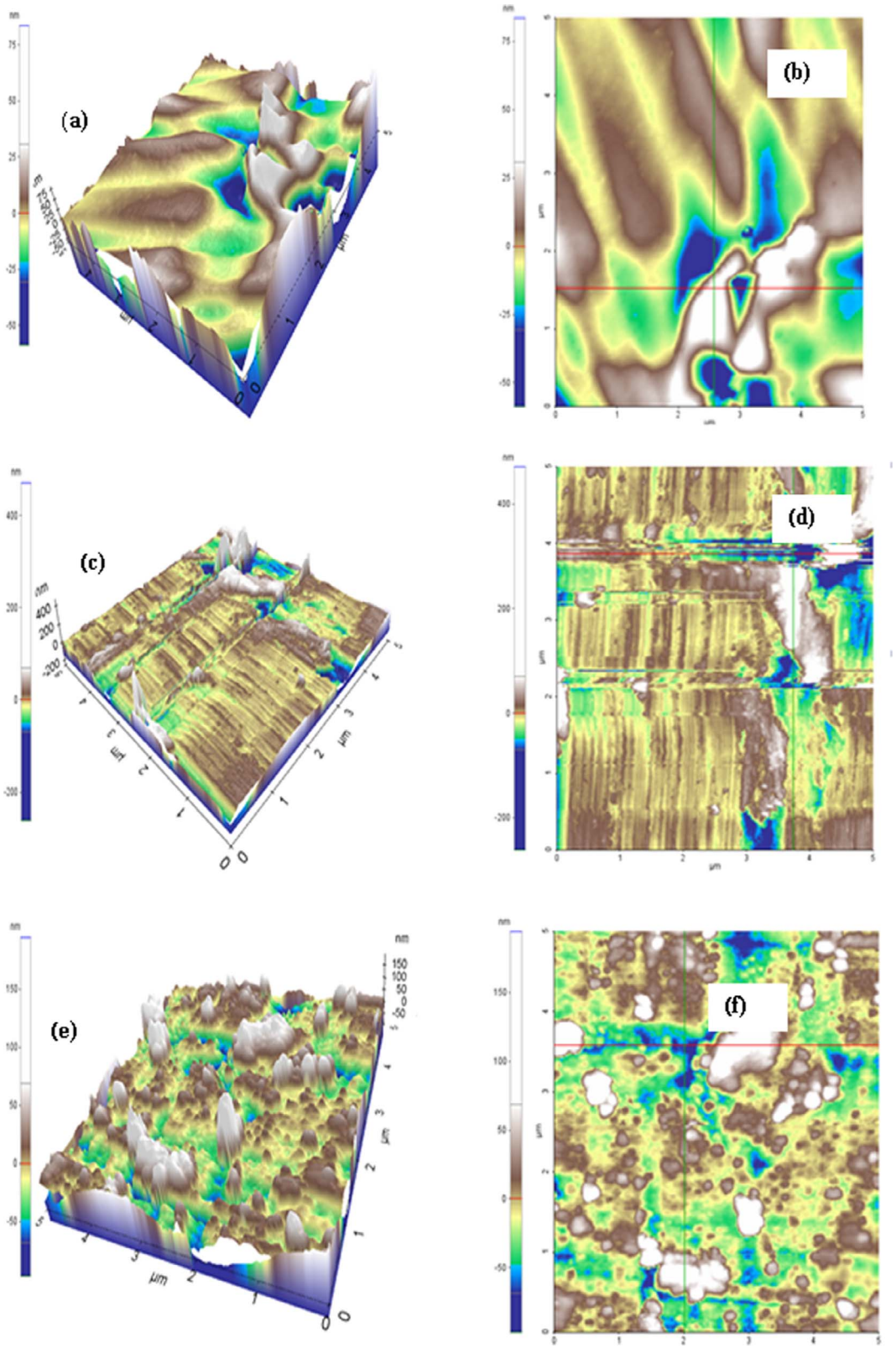

Fig. 7. 3D and 2D AFM images respectively of AA7075-T6 steel (a, b) unexposed, (c, d) exposed to 3.5% NaCl solution, and (e, f) exposed to 3.5% NaCl solution containing 50% EG for 6 h at 25 °C.

chloride ions from the surface and by so doing protect the surface from corrosion. The chloride content on the surface decreased to 4.73% while percentage O increased from 26.04% to 33.93%. The protection occasioned by the adsorption of EG onto the alloy surface is also obvious in the smoother surface in Fig. 6(e) compare to Fig. 6(c). The appearance of C peak in Fig. 6(f) with weight percentage of 0.83% provide experimental evidence to the claim of adsorption of EG onto AA7075-T6 alloy sample.

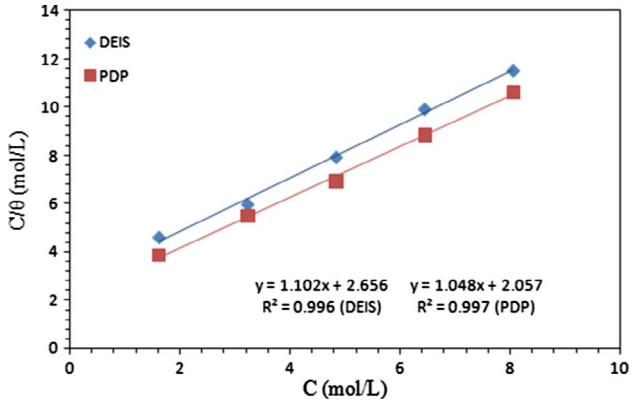

Fig. 8. Langmuir plot of C\θ versus C forAA7075-T6 alloy in 3.5% NaCl solution containing various concentrations of EG at ordinary temperature.

3.3.2. AFM investigations

Fig. 7 presents the 3D and 2D AFM photographs respectively for AA7075-T6 steel (a, b) unexposed, (c, d) exposed to 3.5% NaCl solution, and (e, f) exposed to 3.5% NaCl solution containing 50% EG for 6 h at 25 °C. The portions analyzed are shown in the 2D images with red and green lines. Before experiments (Fig. 7a and b), the R_a (mean of a set of independent measurement of surface peaks and valleys) is between 16.909–20.607 μm while R_z (the root mean square average of profile height deviations from mean line) stands at 55.760–78.926 μm. This values infer a relatively smooth surface. Upon exposure to 3.5% NaCl solution (Fig. 7(c) and (d), the R_a and R_z values increased significantly to 46.241–70.371 μm and 236.950–241.106 μm respectively. As could be seen in Fig. 7(c) and (d), the metal surface is eroded. This agrees with the SEM and experimental results that AA7075-T6 sample was severely damaged in 3.5% NaCl solution. Judging from the R_a (33.073–46.366 μm) and R_z (142.460–173.552 μm) values for the surfaces in Fig. 7(e) and (f), the alloy surface was protected against corrosion in 3.5% NaCl + 50% EG environment.

4. Adsorption investigations

The results from the applied techniques suggest the adsorption of EG molecules on AA7075-T6 surface. There are, however two ways in which organic inhibitor molecules can be adsorbed on a metal surface. The physisorption and chemisorption modes. In physical adsorption, charged inhibitor molecules are held on a metal surface by electrostatic force [29]. In chemisorption, the inhibitor molecules and the metal go into covalent or coordinate bonding [29]. Interestingly, this two modes of adsorption can occur on the same substrate surface [30]. Adsorption isotherm is a useful tool that can provide information on the dominant adsorption mode on a metal surface. Usually, experimental data are manually fitted into adsorption isotherms in order to select the isotherm that best describe the adsorption of inhibitor on a substrate surface. The linear regression coefficient (R^2) is used as a gauge and in literature [21,23,29,30], isotherm plot with R^2 value in the range of 0.900–1.00 is regarded as giving a good fit to experimental data. In our case, the best fit was obtained with Langmuir adsorption isotherm (Fig. 8). The general form of Langmuir isotherm model is given in Eq. (15) [26].

$$\frac{C_{inh}}{\theta} = \frac{1}{K_{ads}} + C_{inh} \tag{15}$$

where C_{inh} is the amount of EG, θ is the surface coverage, and K_{ads} is the equilibrium constant of adsorption-desorption process. The Langmuir adsorption model assumes monolayer adsorption of inhibitor molecules and non interaction of adsorbed inhibitor molecules with each other [31]. By the assumption of non interplay between adsorbed species, the slope of C_{inh}/θ versus C_{inh} should be unity. In Fig. 8, the slope is slightly bigger than one and thus undermine the requirement of Langmuir model. Authors [31–33] have established that bulky molecules adsorbed on metal surface interact with each other. Adsorbed EG molecules may have interacted with each other resulting in the observed slight deviation of the slope from unity.

From the intercept of the DEIS and PDP linear graphs in Fig. 8, the K_{ads} value of 3.04 mol^{-1} and 3.30 mol^{-1} respectively is derived. The obtained K_{ads} value is low and signify weak adsorption of EG molecules on AA7075-T6 surface. The K_{ads} parameter is connected to the standard free energy of adsorption thus [29]:

$$\Delta G^0_{ads} = -RT\ln(55.5K_{ads}) \tag{16}$$

where R is the universal gas constant and T is the absolute temperature. For the investigated system, ΔG^0_{ads} value is −7.53 kJ/mol and −8.16 kJ/mol for DEIS and PDP respectively. The negative sign reflects the possibility of EG molecules adsorption on AA7075-T6 surface. The ΔG^0_{ads} value fall into the category that defines physical adsorption mode. ΔG^0_{ads} value equal to −20 kJ/mol or less indicates physical adsorption mode while value around −40 kJ/mol or more is associated with chemical adsorption [29–31].

5. Conclusion

On the basis of the results of this investigation, the following conclusions are drawn:

(1) The corrosion of AA7075-T6 aluminum alloy in 3.5% NaCl solution is controlled by charge transfer;
(2) In NaCl + EG system, protective layer formed by adsorbed EG molecules alloy corrosion;
(3) Adsorbed EG molecules interfere on both the anodic and cathodic corrosion reactions;
(4) The adsorption of EG molecules onto AA7075-T6 surface is according to Langmuir adsorption model and the mode of adsorption is physisorption;
(5) SEM, EDAX, and AFM results support the claim of EG molecules being adsorbed on AA7075-T6 surface

Acknowledgements

The authors acknowledge the financial support by Duzce University Research Council for Science and Technology (BAP) (Project No.: 2017.06.05.565), Dr. Kazimierz Darowicki and Pawel Slepski for the provision of the DEIS software.

References

[1] U.M.R. Paturi, S.K.R. Narala, R.S. Pundir, Constitutive flow stress formulation, model validation and FE cutting simulation forAA7075-T6aluminumalloy, Mater. Sci. Eng. A 605 (2014) 176–185.
[2] F. Andreatta, M.M. Lohrengel, H. Terryn, J.H.W. de Wit, Electrochemical characterisation of aluminium AA7075-T6 and solution heat treated AA7075 using a micro-capillary cell, Electrochim. Acta 48 (2003) 3239–3247.
[3] S. Dey, M.K. Gunjan, I. Chattoraj, Effect of temper on the distribution of pits in AA7075 alloys, Corros. Sci. 50 (2008) 2895–2901.
[4] W. Tian, S. Li, B. Wang, J. Liu, M. Yu, Pitting corrosion of naturally aged AA 7075 aluminum alloys with bimodal grain size, Corros. Sci. 113 (2016) 1–16.
[5] M. Navaser, M. Atapour, Effect of friction stir processing on pitting corrosion and intergranular attack of 7075 aluminum alloy, J. Mater. Sci. Technol. 33 (2017) 155–165.
[6] W. Tian, S. Li, X. Chen, J. Liu, M. Yu, Intergranular corrosion of spark plasma sintering assembled bimodal grain sized AA7075 aluminum alloys, Corros. Sci. 107 (2016) 211–224.
[7] M. Santambrogio, G. Perrucci, M. Trueba, S.P. Trasatti, M.P. Casaletto, Effect of major degradation products of ethylene glycol aqueous solutions on steel corrosion, Electrochim. Acta 203 (2016) 439–450.
[8] J.E. Bailey, Ullmann's Encyclopedia of Industrial Chemistry, VCH, New York, 2003.
[9] H. Medhashree, A.N. Shetty, Electrochemical corrosion study of Mg–Al–Zn–Mn alloy in aqueous ethylene glycol containing chloride ions, J. Mater. Res. Technol. 6 (1) (2017) 40–49.
[10] A.M. Fekry, M.Z. Fatayerji, Electrochemical corrosion behavior of AZ91D alloy in ethylene glycol, Electrochim. Acta 54 (2009) 6522–6528.
[11] M.N. Khomami, I. Danaee, A.A. Attar, M. Peykari, Corrosion of alloy steel in 30%

ethylene glycol solution and CrO_4^{2-} under hydrodynamic condition, J. Iron. Steel Res. Int. 20 (6) (2013) 82–87.
[12] P. Slepski, K. Darowicki, K. Andrearczyk, On-line measurement of cell impedance during charging and discharging process, J. Electroanaly. Chem. 633 (1) (2009) 121–126.
[13] H.H.H. Hefni, E.M. Azzam, E.A. Badr, M. Hussein, S.M. Tawfik, Synthesis, characterization and anticorrosion potentials of chitosan-g-peg assembled on silver nanoparticles, Int. J. Biol. Macromol. 83 (2016) 297–305.
[14] N. Chaubey, Savita, V.K. Singh, M.A. Quraishi, Corrosion inhibition performance of different bark extracts on aluminium in alkaline solution, J. Assoc. Arab Univ. Basic Appl. Sci. 22 (2017) 38–44.
[15] M.M. Solomon, H. Gerengi, T. Kaya, E. Kaya, S.A. Umoren, Synergistic inhibition of St37 steel corrosion in 15% H2SO4 solution by chitosan and iodide ion additives, Cellulose 24 (2017) 931–950.
[16] N. Yilmaz, A. Fitoz, U¨. Ergun, K.C. Emregul, A combined electrochemical and theoretical study into the effect of2-((thiazole-2-ylimino) methyl) phenol as a corrosion inhibitor for mild steel in a highly acidic environment, Corros. Sci. 111 (2016) 110–120.
[17] M.K. Awad, M.S. Metwally, S.A. Soliman, A.A. El-Zomrawy, M.A. bedair, Experimental and quantum chemical studies of the effect of poly ethylene glycol as corrosion inhibitors of aluminum surface, J. Ind. Eng. Chem. 20 (2014) 796–808.
[18] H. Gerengi, Anticorrosive properties of Date Palm (Phoenix dactylifera L.) fruit juice on 7075 type aluminum alloy in 3.5% NaCl solution, Ind. Eng. Chem. Res. 51 (2012) 12835.
[19] H. Gerengi, H. Goksu, P. Slepski, The inhibition effect of mad honey on corrosion of 2007 type aluminium alloy in 3.5% NaCl solution, Mater. Res. 17 (2014) 255.
[20] Y. Sasikumar, A.S. Adekunle, L.O. Olasunkanmi, I. Bahadur, R. Baskar, M.M. Kabanda, I.B. Obot, E.E. Ebenso, Experimental, quantum chemical and Monte Carlo simulation studies on the corrosion inhibition of some alkyl imidazolium ionic liquids containing tetrafluoroborate anion on mild steel in acidic medium, J. Mol. Liq. 211 (2015) 105–118.
[21] M.M. Solomon, H. Gerengi, S.A. Umoren, Carboxymethyl cellulose/silver nanoparticles composite: Synthesis, characterization and application as a benign corrosion inhibitor for St37 steel in 15% H2SO4 medium, ACS Appl. Mater. Interfaces 9 (2017) 6376–6389.
[22] H. Gerengi, K. Darowicki, P. Slepski, G. Bereket, J. Ryl, Investigation effect of benzotriazole on the corrosion of brass-MM55 alloy in artificial seawater by dynamic EIS, J. Solid State Electrochem. 14 (2010) 897.
[23] S.A. Umoren, M.M. Solomon, U.M. Eduok, I.B. Obot, A.U. Israel, Inhibition of mild steel corrosion in H 2 SO 4 solution by coconut coir dust extract obtained from different solvent systems and synergistic effect of iodide ions: ethanol and acetone extracts, J. Environ. Chem. Eng. 2 (2014) 1048–1060.
[24] J. Liu, D. Wang, L. Gao, D. Zhang, Synergism between cerium nitrate and sodiumdodecylbenzenesulfonate on corrosion of AA5052 aluminium alloy in 3 wt.% NaCl solution, Appl. Surf. Sci. 389 (2016) 369–377.
[25] D. Wang, D. Yang, D. Zhang, K. Li, L. Gao, T. Lin, Electrochemical and DFT studies of quinoline derivatives on corrosioninhibition of AA5052 aluminium alloy in NaCl solution, Appl. Surf. Sci. 357 (2015) 2176–2183.
[26] D. Wang, L. Gao, D. Zhang, D. Yang, H. Wang, T. Lin, Experimental and theoretical investigation on corrosion inhibition of AA5052 aluminium alloy by L-cysteine in alkaline solution, Mater. Chem. Phys. 169 (2016) 142-151.
[27] E.S.M. Sherif, Effects of 3-Amino-1, 2, 4-triazole-5-thiol on the inhibition ofpure aluminum corrosion in aerated stagnant 3.5 wt.% NaCl solution as acorrosion inhibitor, Int. J. Electrochem. Sci. 7 (2012) 4847–4859.
[28] Y. Liu, Y.F. Cheng, Characterization of passivity and pitting corrosion of 3003 aluminum alloy in ethylene glycol–water solutions, J. Appl. Electrochem. 41 (1) (2011) 151–159.
[29] M. Yadav, T.K. Sarkar, I.B. Obot, Indolines as novel corrosion inhibitors: Electrochemical, XPS, DFT and molecular dynamics simulation studies, Corros. Sci. https://doi.org/10.1016/j.corsci.2017.03.002.
[30] M.M. Solomon, S.A. Umoren, Performance evaluationof poly (methacrylic acid) as corrosion inhibitor in the presence of iodide ions for mild steel in H_2SO_4solution, J. Adhes. Sci. Technol. 29 (11) (2015) 1060–1080.
[31] M.M. Solomon, S.A. Umoren, I.I. Udosoro, A.P. Udoh, Inhibitive and adsorption behaviour of carboxymethyl cellulose on mild steel corrosion in sulphuric acid solution, Corros. Sci. 52 (2010) 1317–1325.
[32] M.A. Migahed, H.M. Mohammed, A.M. Al-Sabagh, Corrosion inhibition of H-11 type carbon steel in 1 M hydrochloric acid solution by N-propyl amino lauryl amide and its ethoxylated derivatives, Mater. Chem. Phys. 80 (2003) 169.
[33] A.A. Abdul Azim, L.A. Shalaby, H. Abbas, Mechanism of the corrosion inhibition of Zn anode in NaOH by gelatine and some inorganic anions, Corros. Sci. 14 (1974) 21.